Geophysical Journal International

Empirically determined finite frequency sensitivity kernels for surface waves

Journal:	*Geophysical Journal International*
Manuscript ID:	Draft
Manuscript Type:	Research Paper
Date Submitted by the Author:	
Complete List of Authors:	Lin, Fan-Chi; University of Colorado at Boulder, Physics Ritzwoller, Michael; University of Colorado at Boulder, Department of Physics
Keywords:	Surface waves and free oscillations < SEISMOLOGY, Seismic tomography < SEISMOLOGY, Wave propagation < SEISMOLOGY

Empirically determined finite frequency sensitivity kernels for surface waves

Fan-Chi Lin[1] & Michael H. Ritzwoller[1]

1 – Center for Imaging the Earth's Interior, Department of Physics, University of Colorado at Boulder, Boulder, CO 80309-0390 USA,
linf@ciei.colorado.edu, (303 492 0985)

Abstract

We demonstrate a method for the empirical construction of 2D surface wave phase travel time finite frequency sensitivity kernels by using phase travel time measurements obtained across a large array. The method exploits the virtual source and reciprocity properties of the ambient noise cross-correlation method. The adjoint method is used to construct the sensitivity kernels, where phase travel time measurements for an event (an earthquake or a virtual ambient noise source at one receiver) determine the forward wave propagation and a virtual ambient noise source at a second receiver gives the adjoint wave propagation. The interference of the forward and adjoint waves is then used to derive the empirical kernel. Examples of station-station and earthquake-station empirical finite frequency kernels within the western US based on ambient noise and earthquake phase travel time measurements across USArray stations are shown in order to illustrate the structural effects on the observed empirical sensitivity kernels.

Introduction

Seismic waves with non-infinite (finite) frequencies are sensitive to earth structures away from the geometrical ray. This finite frequency effect is particularly important for surface wave tomography because of the relatively long periods and wavelengths involved, especially in teleseismic applications (Yoshizawa & Kennett, 2002; Zhou et al., 2004; Yang & Forsyth, 2006). Surface wave tomography is often based on ray theory with either straight (e.g., Barmin et al., 2001) or bent (refracted) rays (Lin et al., 2009), and in some cases regularization is introduced to mimic off-ray sensitivity (e.g., Barmin et al., 2001) or approximate analytical sensitivity kernels are applied (e.g., Ritzwoller et al., 2002; Levshin et al., 2005). Surface wave tomography methods based on accurate finite frequency kernels potentially can improve resolution compared to ray theory and resolve sub-wavelength structures. Whether such tomographic methods based on analytical finite frequency kernels derived from a 1D earth model are better than methods using ad hoc kernels remains under debate (e.g., Yoshikawa & Kennett, 2002; van der Hilst & de Hoop, 2005; Montelli et al., 2006; Trampert & Spetzler, 2006).

With advances in computational power and numerical methodology, in particular with the development of the adjoint method (Tromp et al., 2005), increasingly accurate numerical sensitivity kernels based on more realistic 2D and 3D reference models have begun to emerge. The use of these numerical sensitivity kernels in tomographic inversions has also begun to appear (e.g. Peter et al., 2007; Tape et al., 2009). The method remains computationally imposing, however, particularly when the dataset and number of model parameters are large.

In this study, we present an empirical (non-analytical, non-numerical) method to construct 2D phase travel time sensitivity kernels for surface waves across a large array where, in essence, the real earth acts as the reference model. We follow the basic idea of the adjoint method, but instead

of performing a numerical simulation we use the phase travel time measurements across an array of stations to obtain the needed information about wave propagation. In particular, we utilize the virtual source property of ambient noise cross-correlation measurements to obtain information about wave propagation due to an impulsive force at one station location in order to mimic the adjoint simulation in the numerical method. Because spatial interpolations are performed to estimate the phase travel time and the sensitivity kernel on a spatial grid (0.2º×0.2º here), a large-scale high-density array of stations is required. The western US covered by EarthScope USArray stations (Figure 1) is an ideal setting for demonstrating this method. Empirical sensitivity kernels for both ambient noise and telesiesmic earthquakes across USArray are presented and effects of regional phase speed variations (Figure 2) are discussed. Although examples are presented only for Rayleigh waves at periods of 20, 30, and 40 sec, in principle the method is extendable to shorter and longer periods and to Love waves.

The Theoretical Background

A detailed theoretical derivation of the adjoint method to construct a 2D phase travel time sensitivity kernel for surface waves by approximating the surface wave as a membrane wave was presented by Peter et al. (2007). For a fixed event location x_e, the authors showed that the phase time perturbation $\delta\tau$ due to local phase speed perturbations $\delta c(\boldsymbol{x})$ can be linked through a surface integral

$$\frac{\delta\tau}{\tau_0} = \int_\Omega K(\boldsymbol{x}, \boldsymbol{x}_r) \frac{\delta c(\boldsymbol{x})}{c_0(\boldsymbol{x})} d\boldsymbol{x} \quad (1)$$

and the sensitivity kernel $K(x, x_r)$ at field position x can be expressed as

$$K(\boldsymbol{x}, \boldsymbol{x}_r) = -\frac{2}{\tau_0 c_0^2(\boldsymbol{x})} \int_0^T \bar{s}^\dagger(\boldsymbol{x}, \boldsymbol{x}_r, T-t) \partial_t^2 s(\boldsymbol{x}, t) dt, \quad (2)$$

where x_r is the receiver location, τ_0 is the reference phase travel time between the event and the receiver, c_0 is the phase speed for the reference model, T is the duration of the seismogram, $\bar{s}^\dagger$ is the adjoint wavefield, and s is the forward wavefield. The adjoint wavefield $\bar{s}^\dagger$ is the wavefield emitted by an adjoint source $\bar{f}^\dagger$ at the receiver location

$$\bar{f}^\dagger(\boldsymbol{x},t) = \frac{1}{N} w(T-t)\partial_t s(\boldsymbol{x}_r, T-t)\delta(\boldsymbol{x}-\boldsymbol{x}_r), \quad (3)$$

where N is a normalization factor defined by

$$N=\int_0^T w(t)s(\boldsymbol{x}_r,t)\partial_t^2 s(\boldsymbol{x}_r,t)dt \quad (4)$$

and $w(t)$ denotes the cross-correlation time window for the phase travel time measurement.

For a phase travel time at an instantaneous frequency, we simplify the equation for the forward wavefield by assuming that

$$s(\boldsymbol{x},t) = A_s(\boldsymbol{x})\cos(\omega[t-\tau_s(\boldsymbol{x})]) \quad (5)$$

where $A_s(\boldsymbol{x})$ and $\tau_s(\boldsymbol{x})$ are the forward wavefield's amplitude and phase travel time at each location and ω is the angular frequency. Substituting equation (5) into equation (3), the adjoint source $\bar{f}^\dagger$ can be rewritten as

$$\bar{f}^\dagger(\boldsymbol{x},t) = \frac{\omega}{N} w(T-t)A_s(\boldsymbol{x}_r)\sin(\omega[T-t-\tau_s(\boldsymbol{x}_r)])\,\delta(\boldsymbol{x}-\boldsymbol{x}_r). \quad (6)$$

By assuming an infinitely wide time window in which $w(t)=1$ for all t, the adjoint wavefield $\bar{s}^\dagger$ can then be expressed as

$$\bar{s}^\dagger(\boldsymbol{x},\boldsymbol{x}_r,t) = \frac{-\omega}{N} A_s(\boldsymbol{x}_r)A_{\bar{s}^\dagger}(\boldsymbol{x},\boldsymbol{x}_r)\sin(\omega\left[-T+t+\tau_s(\boldsymbol{x}_r)-\tau_{\bar{s}^\dagger}(\boldsymbol{x},\boldsymbol{x}_r)\right]-\tfrac{\pi}{2}), \quad (7)$$

or

$$\bar{s}^\dagger(\boldsymbol{x},\boldsymbol{x}_r,T-t) = \frac{\omega}{N} A_s(\boldsymbol{x}_r)A_{\bar{s}^\dagger}(\boldsymbol{x},\boldsymbol{x}_r)\cos(\omega[-t+\tau_s(\boldsymbol{x}_r)-\tau_{\bar{s}^\dagger}(\boldsymbol{x},\boldsymbol{x}_r)]), \quad (8)$$

where $A_{\bar{s}^\dagger}(\boldsymbol{x},\boldsymbol{x}_r)$ and $\tau_{\bar{s}^\dagger}(\boldsymbol{x},\boldsymbol{x}_r)+\frac{\pi}{2\omega}$ represent the adjoint wavefield amplitude and phase travel time due to an impulsive force with an unit amplitude at the receiver location. The $\frac{\pi}{2}$ phase shift

represents the phase delay between an impulsive force and displacement. Substituting equation (8) into equation (2) and assuming the duration of the seismogram is sufficiently large, the finite frequency sensitivity kernel for an instantaneous frequency ω can be expressed as

$$K_{in}(\boldsymbol{x}, \boldsymbol{x}_r, \omega) = \frac{-2\omega A_{\bar{s}\dagger}(\boldsymbol{x}, \boldsymbol{x}_r)}{\tau_0 c_0^2(\boldsymbol{x})} \left(\frac{A_s(\boldsymbol{x})}{A_s(\boldsymbol{x}_r)}\right) \cos(\omega[\tau_s(\boldsymbol{x}_r) - \tau_{\bar{s}\dagger}(\boldsymbol{x}, \boldsymbol{x}_r) - \tau_s(\boldsymbol{x})]). \quad (9)$$

For a constant speed reference model $c(\boldsymbol{x}) = c_0'$ under the far field approximation, $A_{\bar{s}\dagger}(\boldsymbol{x}, \boldsymbol{x}_r)$, $\tau_{\bar{s}\dagger}(\boldsymbol{x}, \boldsymbol{x}_r)$, $A_s(\boldsymbol{x})$, and $\tau_s(\boldsymbol{x})$ can be derived analytically from the Green's function of the Helmholtz equation as

$$A_{\bar{s}\dagger}(\boldsymbol{x}, \boldsymbol{x}_r) = \sqrt{\frac{1}{8\pi k |\boldsymbol{x} - \boldsymbol{x}_r|}} \quad (10a)$$

$$\tau_{\bar{s}\dagger}(\boldsymbol{x}, \boldsymbol{x}_r) = \frac{|\boldsymbol{x} - \boldsymbol{x}_r|}{c_0'} - \frac{\pi}{4\omega} \quad (10b)$$

$$A_s(\boldsymbol{x}) = \sqrt{\frac{1}{8\pi k |\boldsymbol{x} - \boldsymbol{x}_e|}} \quad (10c)$$

$$\tau_s(\boldsymbol{x}) = \frac{|\boldsymbol{x} - \boldsymbol{x}_e|}{c_0'} - \frac{\pi}{4\omega} \quad (10d)$$

where $k = \frac{\omega}{c_0'}$ is the wave number and $\boldsymbol{x}_e$ is the event location. Substituting these expressions into equation (9) and letting $\tau_0 = \frac{|\boldsymbol{x}_r - \boldsymbol{x}_e|}{c_0'}$, the analytical kernel $K_{in}^a(\boldsymbol{x}, \boldsymbol{x}_r, \omega)$ based on a 1D earth model can be expressed as

$$K_{in}^a(\boldsymbol{x}, \boldsymbol{x}_r, \omega) = \frac{-2\omega}{|\boldsymbol{x}_r - \boldsymbol{x}_e| c_0'} \left(\sqrt{\frac{|\boldsymbol{x}_r - \boldsymbol{x}_e|}{8\pi k |\boldsymbol{x} - \boldsymbol{x}_e||\boldsymbol{x} - \boldsymbol{x}_r|}}\right) \cos(k[|\boldsymbol{x}_r - \boldsymbol{x}_e| - |\boldsymbol{x} - \boldsymbol{x}_r| - |\boldsymbol{x} - \boldsymbol{x}_e|] + \frac{\pi}{4}), \quad (11)$$

which is similar to the 2D analytical phase kernel derived by Zhou et al. (2004) based on a 1D earth model.

Starting from equation (9), the sensitivity kernel for a surface wave between a seismic event and a receiver at an instantaneous frequency at an arbitrary location $\boldsymbol{x}$ can be determined empirically with knowledge of the forward amplitude $A_s(\boldsymbol{x})$, forward phase travel time $\tau_s(\boldsymbol{x})$, adjoint amplitude $A_{\bar{s}^\dagger}(\boldsymbol{x}, \boldsymbol{x}_r)$, adjoint phase travel time $\tau_{\bar{s}^\dagger}(\boldsymbol{x}, \boldsymbol{x}_r)$, the local phase speed $c_0(\boldsymbol{x})$, and the forward wavefield's amplitude $A_s(\boldsymbol{x}_r)$ and phase travel time $\tau_s(\boldsymbol{x}_r)$ measured at the receiver location. Among these parameters, the three phase travel time terms control the "phase", the cosine term in equation (9) of the sensitivity kernel, which varies between -1 and +1, while the other terms control the "amplitude" of the sensitivity kernel. The shape of the sensitivity kernel is determined solely by the phase term such that regions of positive and negative sensitivities are separated by the null lines, where the cosine term vanishes. In this study, we empirically determine this cosine term and, therefore, the shape of the sensitivity kernel by replacing $\tau_s(\boldsymbol{x}_r)$ with the phase travel time measurement for the forward wavefield at the receiver, $\tau_s(\boldsymbol{x})$ with the forward wavefield's phase travel time measurements across the USArray, and $\tau_{\bar{s}^\dagger}(\boldsymbol{x}, \boldsymbol{x}_r)$ with the phase travel time measurements between the receiver to all other location across the USArray using ambient noise cross-correlation measurements. Although the local phase speed can be estimated fairly well through tomography inversions, such as the isotropic speed maps shown in Figure 2, and amplitudes can be measured for earthquake events, the amplitude information is typically lost for ambient noise measurements due to the time and frequency domain normalizations that are applied during data processing (e.g., Bensen et al., 2007). Thus, we will assume that both the forward and adjoint amplitudes are governed by geometrical spreading for a constant speed $c_0^{'}$ reference model (equation (10b) and (10d)) and will also assume that $c_0(\boldsymbol{x}) = c_0^{'} = \frac{|\boldsymbol{x}_r - \boldsymbol{x}_e|}{\tau_s(\boldsymbol{x}_r) + \frac{\pi}{4\omega}}$.

In this case, for $\tau_0 = \frac{|\boldsymbol{x}_r - \boldsymbol{x}_e|}{c_0'} = \tau_s(\boldsymbol{x}_r) + \frac{\pi}{4\omega}$, equation (9) can be written for an empirical sensitivity kernel as

$$K_{in}^{e}(\boldsymbol{x}, \boldsymbol{x}_r, \omega) = \frac{-2\omega}{|\boldsymbol{x}_r - \boldsymbol{x}_e| c_0'} \left(\sqrt{\frac{|\boldsymbol{x}_r - \boldsymbol{x}_e|}{8\pi k\, |\boldsymbol{x} - \boldsymbol{x}_e||\boldsymbol{x} - \boldsymbol{x}_r|}} \right) \cos(\omega[\tau_s(\boldsymbol{x}_r) - \tau_{\bar{s}^\dagger}(\boldsymbol{x}, \boldsymbol{x}_r) - \tau_s(\boldsymbol{x})]). \quad (12)$$

Here again, $k = \frac{\omega}{c_0'}$ but all variables are now measurable quantities. When lateral wave speed variations are small, it is likely that this will be a good approximation to the sensitivity kernel. In the presence of strong lateral wave speed variations, focusing and defocusing may affect the amplitude term in equation (9) significantly, but the phase of kernel (its shape) should continue to be accurate.

Equations (11) and (12) are analytical and empirical kernels, respectively, for an instantaneous frequency. Phase travel time measurements at frequency ω_0 typically are obtained within a finite band-width in which a band-pass filter $g(\omega, \omega_0)$ has been applied, so that instantaneous kernels are not entirely appropriate. In this case, the forward wavefield $s(\boldsymbol{x}, t)$ in equation (5) can be replaced by

$$s(\boldsymbol{x}, t) = \int g(\omega, \omega_0) A_s(\boldsymbol{x}) \cos(\omega[t - \tau_s(\boldsymbol{x})]) d\omega \quad (13)$$

and the finite band-width analytical $K_{fb}^{a}(\boldsymbol{x}, \boldsymbol{x}_r, \omega_0)$ and empirical $K_{fb}^{e}(\boldsymbol{x}, \boldsymbol{x}_r, \omega_0)$ sensitivity kernels can be expressed as

$$K_{fb}^{a,e}(\boldsymbol{x}, \boldsymbol{x}_r, \omega_0) = \frac{\int g(\omega, \omega_0)^2 K_{in}^{a,e}(\boldsymbol{x}, \boldsymbol{x}_r, \omega) d\omega}{\int g(\omega, \omega_0)^2 d\omega}, \quad (14)$$

where $K_{in}^{a}(\boldsymbol{x}, \boldsymbol{x}_r, \omega)$ and $K_{in}^{e}(\boldsymbol{x}, \boldsymbol{x}_r, \omega)$ are the analytical and empirical sensitivity kernels for an instantaneous frequency ω given by in equations (11) and (12).

Methods and Results

We follow closely the ambient noise data processing method described by Lin et al. (2008) to obtain the Rayleigh wave phase travel time between each USArray station pair. For each station – referred to as the "center station" -- all phase travel time measurements larger than 1 period between that station and all other stations with a SNR > 15 (Bensen et al., 2007) are used to determine the phase travel time map on a 0.2º×0.2º grid by minimum curvature fitting. Near each center station, where phase travel times are smaller than 1 period, a linear interpolation is performed by fixing the phase travel time to zero at the center station location. We follow the criteria of Lin et al. (2009) to select the regions with reliable phase travel times. Two examples of 30 sec period Rayleigh wave phase travel time maps with center stations G06A and R10A are shown in Figure 3a-b. These phase travel time maps are the basis for the eikonal tomography method presented by Lin et al. (2009).

To obtain the station-station empirical finite frequency sensitivity kernel for ambient noise applications, the phase travel time maps for each of the two center stations are used to measure the parameters in equation (12). For each field position x, we compute the forward phase time $\tau_s(\boldsymbol{x})$ and adjoint phase time $\tau_{\bar{s}^\dagger}(\boldsymbol{x}, \boldsymbol{x}_r)$ from the values of the two phase travel maps. Due to the event-receiver symmetry in equation (12), which station is considered as the event and which station is considered as the receiver is irrelevant.

Figure 3c shows the 30 sec instantaneous frequency Rayleigh wave empirical finite frequency kernel between USArray stations G06A and R10A constructed based on the phase travel time maps shown in Figure 3a-b. The analytical kernel derived from equation (11) assuming $c_0' = \frac{|\boldsymbol{x}_e - \boldsymbol{x}_r|}{\tau_s(\boldsymbol{x}_r) + \frac{\pi}{4\omega}}$ is shown in Figure 3d for comparison. Using c_0' from the empirical kernel in the analytical kernel minimizes the differences caused by the reference wave speed. In general, the

empirical and analytical kernels agree well for this path, which is because of the relatively homogeneous phase velocity distribution between these two stations at this period (Figure 2b).

Figures 3e and 3f show an example of the 30 sec finite band-width empirical and analytical kernels between stations G06A and R10A. In order to mimic the filter applied by our frequency-time phase velocity measurement method (e.g., Lin et al., 2007), we insert the Gaussian band-pass filter $g(\omega,\omega_0) = e^{-\left[\frac{4.3(\omega-\omega_0)}{\omega_0}\right]^2}$ into equation (14), where $\omega_0 = \pi/15$ is the center frequency of the filter. For simplicity of calculation, the phase travel times $\tau_s(\boldsymbol{x}_r)$, $\tau_{\bar{s}^\dagger}(\boldsymbol{x},\boldsymbol{x}_r)$, and $\tau_s(\boldsymbol{x})$ at 30 sec period are used across frequency to estimate the instantaneous frequency kernel. Far from the great-circle path, the sensitivity is weaker for the finite-band width kernels (Figure 3e-f) than for the instantaneous frequency kernels (Figure 3b-c) due to the destructive interference of sensitivity over the frequency band. The finite band-width kernels represent a more realistic sensitivity to the measurement. Although finite band-width kernels should be preferred to compute travel times or in tomographic inversions, instantaneous frequency kernels do not depend on the choice of the band-pass filter and, therefore, are used here in the remainder of this paper.

Figure 4 presents more examples of instantaneous frequency empirical and analytical sensitivity kernels at 20 and 40 sec periods for a different station pair, USArray stations L04A and GSL. For this pair of stations there are generally faster phase speeds on the western side of the great circle path between the stations (Figure 2a, c). East-west phase speed contrasts are, however, stronger at 20 sec period than at 40 sec. Clear differences are observed between the empirical and analytical sensitivity kernels at 20 sec period (Figure 4a-b), where the empirical kernel is not only broader but also is shifted toward the western (faster) side. Kernel cross-sections at the mid-distance from the two stations are shown in Figure 4c, in which an east-west asymmetry across

the great circle path is clearly apparent for the empirical sensitivity kernel. The differences between the empirical and analytical kernels can be qualitatively understood by the principle of least-time, in which waves tend to travel through regions with faster phase speeds and are, therefore, also more sensitive to it. At 40 sec period, the differences between the empirical and analytical kernels (Figure 4d-e) are less pronounced due to the reduced east-west phase speed contrast. Nevertheless, asymmetry can still be observed in the mid-distance cross-section (Figure 4f). Note that errors in the phase travel time measurements can generate small-scale distortions in the empirical finite frequency kernels, as irregularities in Figures 4a and 4d attest. Only the large-scale features of the empirical kernels are robust. In principle, station-station empirical kernels computed from ambient noise can be used to compute travel times or can be applied in a tomographic inversion, but such applications remain the subject of investigation.

It is also possible to construct the empirical finite frequency sensitivity kernels within an array for surface waves emitted by an earthquake within or outside the array. The 40 sec period Rayleigh wave emitted by a magnitude 6.2 earthquake on September 6th 2007 near Taiwan region is used in Figure 5 as an example of an empirical finite frequency kernel for a teleseismic earthquake. Similar to ambient noise measurements, we first construct the Rayleigh wave phase travel time map for the earthquake by using all phase travel time measurements across the USArray stations (Figure 5b). To construct the empirical kernel between the earthquake and USArray station X15A within the footprint of the USArray, the 40 sec period Rayleigh wave phase travel time map for X15A (Figure 5c) is used to obtain the adjoint phase travel time $\tau_{\bar{s}^\dagger}(\boldsymbol{x}, \boldsymbol{x}_r)$ at each location. For each location, we substitute $\tau_s(\boldsymbol{x})$ and $\tau_{\bar{s}^\dagger}(\boldsymbol{x}, \boldsymbol{x}_r)$ with the values of the forward and adjoint phase travel time maps, respectively. Although it is possible to

measure forward amplitude $A_s(\boldsymbol{x})$ at each location for earthquakes, we approximate the amplitude by using equations (10c) for the sake of simplicity.

Figure 5d presents the resulting empirical earthquake-station sensitivity kernel and Figure 5e shows the analytical kernel derived from equation (11), again assuming $c_0' = \frac{|\boldsymbol{x}_e - \boldsymbol{x}_r|}{\tau_s(\boldsymbol{x}_r) + \frac{\pi}{4\omega}}$. The earthquake-station empirical finite frequency kernel across the USArray is clearly quite different from the analytical kernel with the center of the kernel rotated approximately 20º to the south. Due to the thin oceanic crust, Rayleigh waves across oceanic basins at 40 sec period have higher phase speeds compared with a global average or to continental areas. The observed Rayleigh wave, therefore, propagates further out into the Pacific basin than predicted by the great-circle ray (Figure 5a). For earthquakes outside an array the empirical kernels are only determined within the footprint of the array. For earthquakes within an array the earthquake-station empirical kernels would be fully determined.

Discussion and Conclusion

In this study, we present a method to construct empirical 2D finite frequency surface wave sensitivity kernels. We show that by mapping the phase travel time observed across a large array and utilizing the virtual source property of ambient noise cross-correlation measurements, the adjoint method can be applied to construct sensitivity kernels within the array without numerical simulations. We show that empirical kernels for both ambient noise and earthquake measurements with sources within or outside the array can be constructed within the footprint of the observing array. Because all phase travel times are measured via surface waves propagating on the earth, the empirical kernels represent the sensitivity of surface waves in which the real

earth acts as the reference model. Significant differences exist between the empirical kernels and analytical kernels derived with a 1D earth model in regions with large lateral wave speed variations.

The complete specification of the empirical kernels requires both phase and the amplitude information about the forward and adjoint wavefields. While efforts are still underway to retrieve amplitude information from the empirical Green's function constructed from ambient noise, geometric spreading is likely to be the principal factor in detemining amplitude variations for wavefields emitted by a source within the array. For teleseismic sources, however, amplitude variations within the array can be strongly perturbed by multipathing. When such effects become important, using the amplitude measurements obtained on real data to replace $A_s(\boldsymbol{x})$ and $A_s(\boldsymbol{x_r})$ in equation (9) should give a better estimate of the "amplitude" part of the empirical kernel.

Using the empirical kernels and equation (1) to predict the phase travel time requires information about real earth structure $c_0(\boldsymbol{x})$, which is generally unknown. By replacing $c_0(\boldsymbol{x})$ by a reference model, the use of the empirical kernel or perhaps preferably the average of the empirical and analytical kernels should improve the accuracy of the phase travel times predicted with the kernel compared to using the analytical kernel alone. Recently, we presented a surface wave tomography method, called eikonal tomography (Lin et al., 2009), that measures phase velocities by calculating the gradient of the phase travel time maps at each spatial location. Whether and how the construction of the empirical finite frequency sensitivity kernels can be applied to improve this method of tomography is still under investigation.

Acknowledgements

Instruments [data] used in this study were made available through EarthScope (www.earthscope.org; EAR-0323309), supported by the National Science Foundation. The facilities of the IRIS Data Management System, and specifically the IRIS Data Management Center, were used for access to waveform and metadata required in this study. The IRIS DMS is funded through the National Science Foundation and specifically the GEO Directorate through the Instrumentation and Facilities Program of the National Science Foundation under Cooperative Agreement EAR-0552316. This work has been supported by NSF grants EAR-0711526 and EAR-0844097. Lin, F. acknowledges a scholarship from SEG Foundation.

References

Barmin, M.P., Ritzwoller, M.H. & Levshin, A.L., 2001. A fast and reliable method for surface wave tomography, *Pure Appl. Geophys.,* 158(8), 1351 - 1375.

Bensen, G. D., Ritzwoller, M. H., Barmin, M. P., Levshin, A. L., Lin, F., Moschetti, M. P., Shapiro, N. M. & Yang, Y., 2007. Processing seismic ambient noise data to obtain reliable broad-band surface wave dispersion measurements, *Geophys. J. Int.,* 169(3), 1239–1260.

Levshin, A.L., Barmin, M.P., Ritzwoller, M.H. & Trampert, J., 2005. Minor-arc and major-arc global surface wave diffraction tomography, *Phys. Earth Planet. Ints.*, 149, 205-223.

Lin, F., Moschetti, M. P. & Ritzwoller, M. H., 2008. Surface wave tomography of the western United States from ambient seismic noise: Rayleigh and Love wave phase velocity maps, *Geophys. J. Int.,* 173(1), 281–298.

Lin, F., Ritzwoller, M. H. & Snieder, R., 2009. Eikonal tomography: surface wave tomography by phase front tracking across a regional broad-band seismic array, *Geophys. J. Int.,* 177(3), 1091–1110.

Montelli, R., Nolet, G. & Dahlen, F.A., 2006. Comment on 'Bananadoughnut kernels and mantle tomography' by van der Hilst and de Hoop, *Geophys. J. Int.,* 167, 1204–1210.

Peter, D., Tape, C., Boschi, L. & Woodhouse, J. H., 2007. Surface wave tomography: Global membrane waves and adjoint methods, *Geophys. J. Int.*, 171, 1098–1117.

Ritzwoller, M.H., Shapiro, N.M., Barmin, M.P. & Levshin, A.L., 2002. Global surface wave diffraction tomography, *J. Geophys. Res.*, 107(B12), 2335.

Tape, C., Liu, Q., Maggi, A. & Tromp, J., 2009. Adjoint tomography of the Southern California crust, *Science*, 325 , 988–992.

Trampert, J. & Spetzler, J., 2006. Surface wave tomography: finite frequency effects lost in the null space, *Geophys. J. Int.,* 164, 394–400.

Tromp, J., Tape, C. & Liu, Q., 2005. Seismic tomography, adjoint methods, time reversal and banana-doughnut kernels, *Geophys. J. Int.*, 160, 195–216.

Van Der Hilst, R.D. & de Hoop, M.V., 2005. Banana-doughnut kernels and mantle tomography, *Geophys. J. Int.,* 163, 956–961.

Yang, Y.J. & Forsyth D.W., 2006. Regional tomographic inversion of the amplitude and phase of Rayleigh waves with 2-D sensitivity kernels, *Geophys. J. Int.,* **166**, 1148-1160.

Yoshizawa,K. & Kennett, B.L.N., 2002. Determination of the influence zone for surface wave paths, *Geophys. J. Int.,* 149, 441–454.

Zhou, Y., Dahlen, F.A. & Nolet, G., 2004. Three-dimensional sensitivity kernels for surface wave observables, *Geophys. J. Int.,* 158, 142–168.

Figure Captions

Figure 1. The USArray Transportable Array stations used in this study.

Figure 2. The (a) 20 sec, (b) 30 sec, and (c) 40 sec period Rayleigh wave phase speed maps determined from all available vertical–vertical component ambient noise cross-correlations between October 2004 and August 2009 across USArray. The eikonal tomography method (Lin et al., 2009) is used to construct these maps. The stations used in Figures 3 and 4 to construct the station-station empirical kernels are also shown.

Figure 3. (a) An example 30 sec Rayleigh wave phase travel time surface for a virtual source located at USArray station G06A (star) based on ambient noise cross-correlations. The triangles indicate the stations with good phase travel time measurements. The blue contours of travel times are separated by 30 sec. (b) Same as (a), but with USArray station R10A (star) as the virtual source. (c) The 30 sec period Rayleigh wave instantaneous frequency empirical finite frequency kernel for the USArray G06A-R10A station-pair constructed from (a) and (b). The line connecting the two stations is the great-circle path. (d) Same as (c), but with the analytical kernel derived with a constant phase speed reference model. (e)-(f) Same as (c) and (d) but with finite band width empirical and analytical kernels, respectively.

Figure 4. (a) The 20 sec period Rayleigh wave empirical finite frequency kernel for the USArray station pair L04A-GSC. The A-B dashed line indicates the mid-distance cross section shown in (c). (b) Same as (a), but the analytical kernel is shown. (c) The mid-distance cross section of the sensitivity kernels shown in (a) and (b). (d)-(f) Same as (a)-(c), but for the 40 sec period Rayleigh wave.

Figure 5. (a) The location of the September 6th 2007 Taiwan earthquake (star), the location of USArray station X15A (triangle), and the great-circle path in between (solid line). (b) The 40 sec Rayleigh wave phase travel time surface for the Taiwan event shown in (a) observed across the USArray. The triangles indicate the stations deemed to have good phase travel time

measurements. Blue contours of travel time are separated by 40 sec. (c) Same as Figure 3a, but for 40 sec Rayleigh wave with USArray station X15A (star) at the virtual source position. (d) The 40 sec period Rayleigh wave empirical finite frequency kernel for the Taiwan event and USArray station X15A constructed from (b) and (c). The triangle indicates the location of the station and the dashed line indicates the great-circle path between the Taiwan event and the station. (e) Same as (d), but with the analytical kernel derived using a constant phase speed reference model.

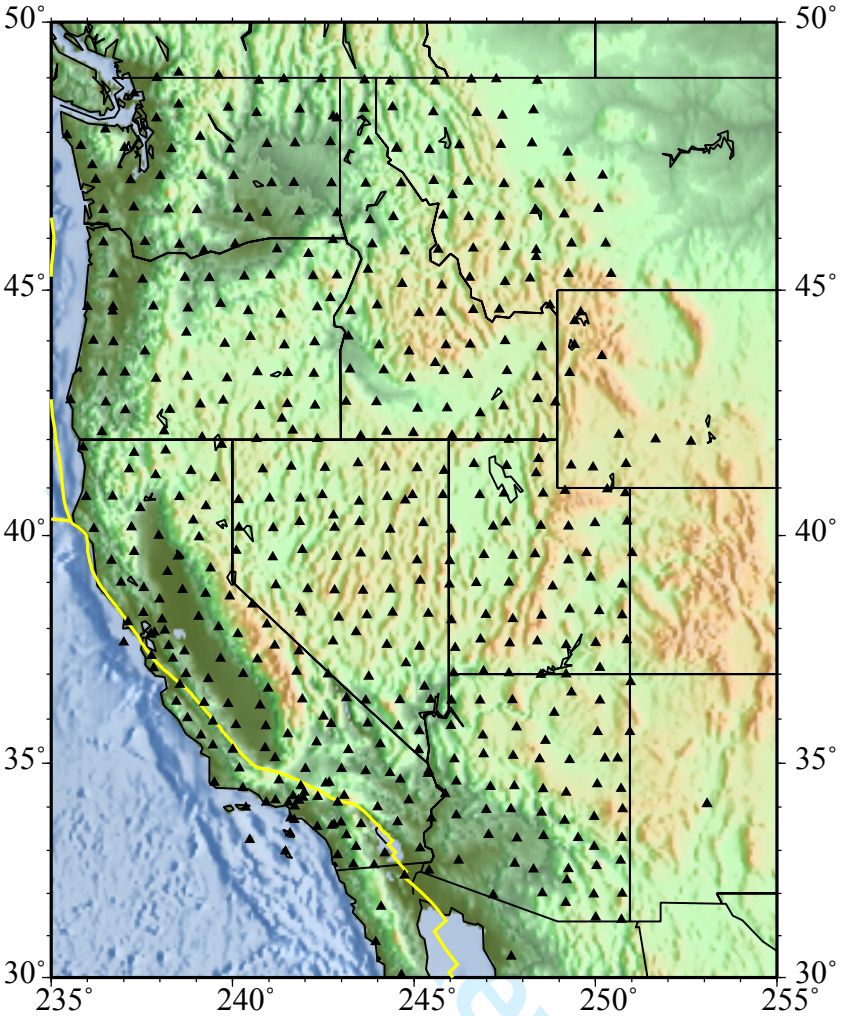

Figure 1

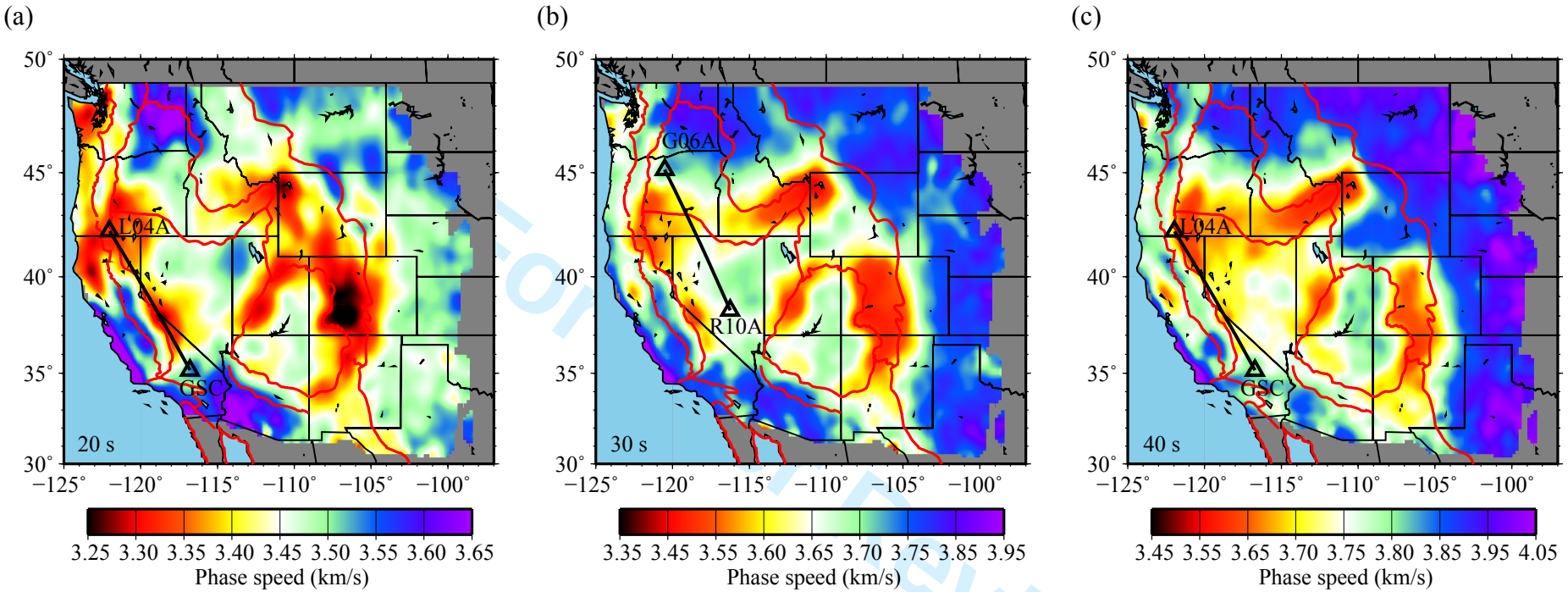

Figure 2

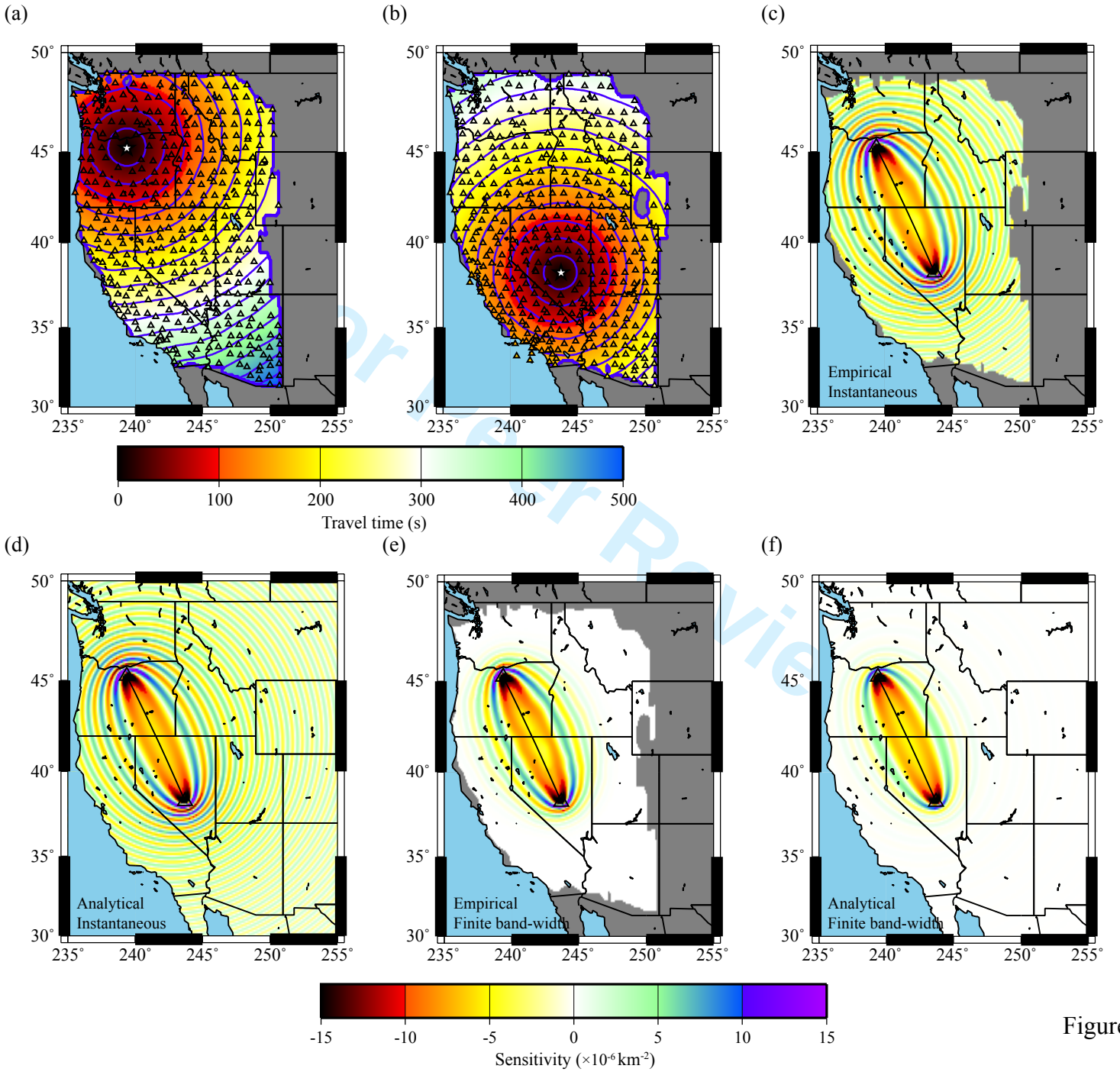

Figure 3

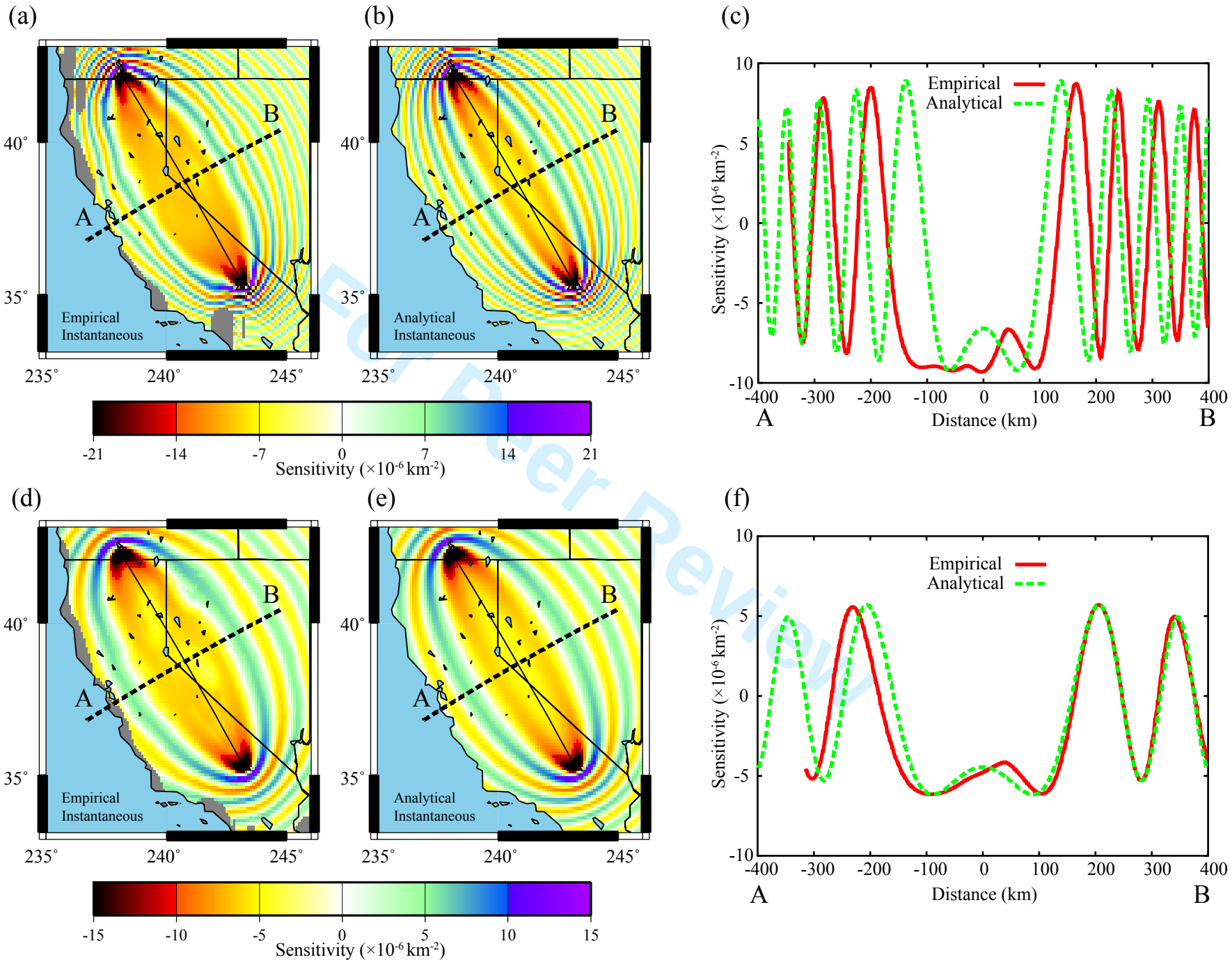

Figure 4

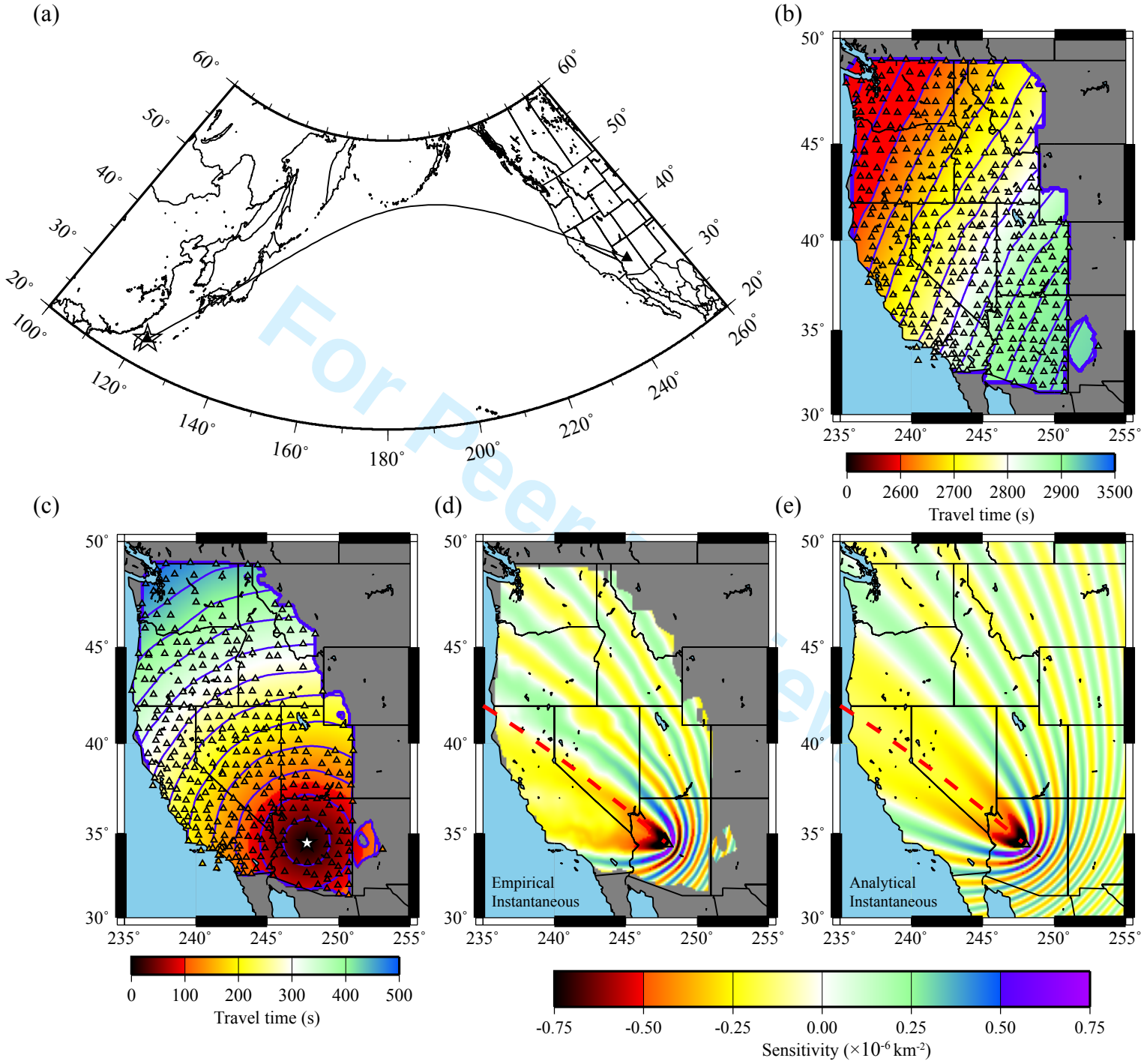

Figure 5